Published in Wear, (2008)

http://dx.doi.org/10.1016/j.wear.2007.10.001

Taguchi method applied to parametric appraisal of erosion behavior of GF-reinforced polyester composites

S.S. Mahapatra[a], **, Amar Patnaik**[b], [1], **and Alok Satapathy**[a], [2],

ssm@nitrkl.ac.in

[a]Department of Mechanical Engineering, National Institute of Technology, Rourkela 769008 India

[b]Department of Mechanical Engineering, National Institute of Technology, Hamirpur 177 005 India

Received 20 February 2007; revised 9 August 2007; accepted 8 October 2007.

Available online 26 November 2007.

Abstract

Polyester composites reinforced with three different weight fractions of woven E-glass fiber reinforcement are developed. To study the effect of various operational and material parameters on erosive wear behavior of these composites in an interacting environment erosion tests are carried out. For this purpose, air jet type erosion test rig and the design of experiments approach utilizing Taguchi's orthogonal arrays are used. The findings of the experiments indicate that the rate of erosion of composites by impact of solid erodent is greatly influenced by the control factors. An optimal parameter combination is

determined, which leads to minimization of erosion rate. Analysis of variance (ANOVA) is performed on the measured data and S/N (signal to noise) ratios. A correlation derived from the results of Taguchi experimental design is proposed as a predictive equation for estimation of erosion wear rate of these composites. It is demonstrated that the predicted results obtained using this equation are consistent with experimental observations. Finally, optimal factor settings for minimum wear rate are determined using genetic algorithm.

Keywords: Erosion rate; GF-polyester composites; Taguchi method; ANOVA: Genetic algorithm

Article Outline

1. Introduction

Solid particle erosion is a general term used to describe mechanical degradation (wear) of any material subjected to a stream of erodent particles impinging on its surface. The effect of solid particle erosion has been recognized by Wahl et al. [1] for a long time. Damage caused by erosion has been reported in several industries for a wide range of situations. Examples have been cited for transportation of airborne solids through pipes by Bitter [2], boiler tubes exposed to flyash by Raask [3] and gas turbine blades by Hibbert and Roy [4]. Solid particle erosion is the progressive loss of original material from a solid surface due to mechanical interaction between the surface and impinging particles. Various applications of polymers and their composites in erosive wear situations are reported by Pool et al.[5], Kulkarni et al. [6] and Aglan et al. [7] in the literature. But solid particle erosion of polymers and their composites has not been investigated to the same extent as for metals or ceramics. However, a number of researchers Barkoula et al.[8], Tewari et al. [9] have evaluated the resistance of various types of polymers and their composites to solid particle erosion. It is widely recognized that polymers and their composites have poor erosion resistance. Their erosion rates (Er) are considerably higher than metals. Also, it is well known that the erosion rate of polymer composites is even higher than that of neat polymers as reported by Häger et al. [10]. The solid particle erosion behavior of polymer composites as a function of fiber content has been studied to a limited extent by investigators like Miyazaki and Takeda [11]. Tilly and Sage [12] have investigated the influence of velocity, impact angle, particle size and weight of impacted abrasives on nylon, carbon-fiber-reinforced nylon, epoxy resin, polypropylene and glass-fiber-reinforced plastic.

Lindsley and Marder [13] found impact velocity (v) to be a critical test variable in erosion, and that it can easily over shadow changes in other variables, such as target material, impact angle etc. Sundararajan and Roy [14] suggested that in addition to velocity, solid particle erosion is governed by the impact angle, particle size, particle shape and hardness. The impact of above parameters has been studied independently keeping all parameters at fixed levels. Therefore, visualization of impact of various factors in an interacting environment really becomes difficult. To this end, an attempt has been made to analyze the impact of more than one parameters on solid particle erosion of PMCs, because in actual practice the resultant erosion rate is the combined effect of impact of more than one interacting variables. An inexpensive and easy-to-operate experimental strategy based on Taguchi's parameter design has been adopted to study effect of various parameters and their interactions. This experimental procedure has been successfully applied by Mahapatra and Patnaik [15, 16, 17, 18, 19, 20] for parametric appraisal in wire electrical discharge machining (WEDM) process, drilling of metal matrix composites, and erosion behavior of metal matrix composites. Successful implementation of Taguchi's design has also been reported by Patnaik et. al.[21] for study of erosion characteristics of polymer composites.

The aim of the present study is, therefore, to investigate the erosion behavior of polyester matrix composites based on Taguchi method under various testing conditions. Further more, the analysis of variance are employed to determine the most significant control factors and their interactions. Finally, an evolutionary approach known as genetic algorithm has been applied for determining optimal factor settings to minimize the erosion rate.

2. Experimental details

2.1 Specimen Preparation

Cross plied E-glass fibers (360 roving taken from Saint Govion) are reinforced in unsaturated isophthalic polyester resin (supplied by Ciba-Giegy Ltd. India) to prepare the composites. The composite slabs are made by conventional hand-lay-up technique. 2% cobalt nephthalate (as accelerator) is mixed thoroughly in isophthalic polyester resin and then 2% methyl-ethyl-ketone-peroxide (MEKP) as hardener is mixed in the resin prior to reinforcement. E-glass fiber and polyester resin have modulus of 72.5 GPa and 3.25 GPa respectively and possess density of 2.59 gm/cc and 1.35 gm/cc respectively. Three composites of different glass fiber weight fractions (30 wt%, 40 wt% and 50 wt%) are fabricated. The castings are put under load for about 24 hours for proper curing at room temperature. Specimens of suitable dimension are cut using a diamond cutter for mechanical characterization and erosion test.

2.2 Test apparatus

Figure 1 shows the schematic diagram of erosion test rig confirming to ASTM G 76. The set up is capable of creating reproducible erosive situations for assessing erosion wear resistance of the prepared composite samples. It consists of an air compressor, an air particle mixing chamber and an accelerating chamber. Dry compressed air is mixed with the particles which are fed at constant rate from a sand flow control knob through the nozzle tube and then accelerated by passing the mixture through a convergent brass nozzle of 3 mm internal diameter. These particles impact the specimen which can be held at various angles with respect to the direction of erodent flow using a swivel and an adjustable sample clip. The velocity of the eroding particles is measured using double

disc method [7]. In the present study, dry silica sand (angular) of different particle sizes (450μm, 600 μm and 800 μm) is used as erodent. Each sample is cleaned in acetone, dried and weighed to an accuracy of ± 0.1 mg using a precision electronic balance. It is then eroded in the test rig for 10 minutes and weighed again to determine the weight loss. The process is repeated till the erosion rate attains a constant value called steady state erosion rate. The ratio of this weight loss to the weight of the eroding particles causing the loss is then computed as a dimensionless incremental erosion rate. The erosion rate is defined as the weight loss of the specimen due to erosion divided by the weight of the erodent causing the loss.

2.3 Mechanical characterization

Micro-hardness measurement is done using a Leitz micro-hardness tester equipped with a square based pyramidal (angle 136^0 between opposite faces) diamond indenter by applying a load of 24.54 N. The tensile test is performed on flat dog-bone shaped composite specimens as per ASTM D 3039-76 test standards using a universal testing machine Instron 1195. Three point bend test is conducted in the same machine at a crosshead speed of 10mm/min to evaluate the flexural strength of the composites. Finally, the eroded surfaces of some selected samples are examined by scanning electron microscope JEOL JSM-6480LV.

2.4 Experimental Design

It has been observed that the erosion rate is influenced by a large number of process parameters (factors) such as impact velocity, impingement angle, fiber loading, erodent size and stand-off distance. Out of all these factors, velocity predominantly governs the rate of erosion. However, the interaction of velocity in the presence of other

factors has not been studied adequately. Hence, it is desirable to study the interaction effect of velocity with other important factors. To this end, Taguchi's parameter design approach is employed for modeling and analyzing the influence of control factors on performance output. The most critical aspect in design of experiment is the selection of control factors. Therefore, a large number of factors are included initially and experiments are conducted to ascertain non-significant factors at the earliest opportunity**.** The operating conditions under which erosion tests are carried out are given in Table 1. The tests are conducted as per experimental design shown in Table 2 at room temperature. Five parameters viz., impact velocity, impingement angle, fiber loading, erodent size and stand-off distance, each at three levels, are considered in this study in accordance with L_{27} (3^{13}) orthogonal design. In Table 2, each column represents a test parameter and a row gives a test condition which is nothing but combination of parameter levels. Five parameters each at three levels would require 3^5 = 243 runs in a full factorial experiment, whereas Taguchi's factorial experiment approach reduces it to 27 runs only offering a great advantage.

The experimental observations are transformed into a signal-to-noise (S/N) ratio. There are several S/N ratios available depending on the type of characteristics. The S/N ratio characteristics can be divided into three categories given by Eqs. (1)- (3) when the characteristic is continuous.

Smaller is the better characteristic: $\frac{S}{N} = -10 \log \frac{1}{n}\left(\sum y^2\right)$ (1)

Nominal the better characteristics: $\frac{S}{N} = -10 \log \frac{1}{n}\left(\sum \frac{\bar{Y}}{S_Y^2}\right)$ (2)

Larger the better characteristics : $\frac{S}{N} = -10 \log \frac{1}{n}\left(\sum \frac{1}{y^2}\right)$ (3)

where $\bar{Y}$ is the average of observed data, S_Y^2 the variation of y, n the number of observations, and y the observed data. “Lower is better” (LB) characteristic with the above S/N ratio transformation is suitable for minimization of erosion rate. A standard linear graph, as shown in Figure 2, is used to assign the factors and interactions to various columns of the orthogonal array [22, 23].

The plan of the experiments is as follows: the first column is assigned to impact velocity (A), the second column to impingement angle (B), the fifth column to fiber loading (C), the eighth column to erodent size (D) and eleventh column to stand-off distance (E), the third and fourth columns are assigned to $(A\times B)_1$ and $(A\times B)_2$ respectively to estimate interaction between impact velocity (A) and impingement angle (B), the sixth and seventh columns are assigned to $(A\times C)_1$ and $(A\times C)_2$ respectively to estimate interaction between the impact velocity (A) and fiber loading (C), the ninth and tenth columns are assigned to $(A\times D)_1$ and $(A\times D)_2$ respectively to estimate interaction between the impact velocity (A) and erodent size (D), the twelfth and thirteenth columns are assigned to $(A\times E)_1$ and $(A\times E)_2$ respectively to estimate interaction between the impact velocity (A) and stand-off distance (E).

3. Results and Discussion

3.1 Mechanical properties

Figure 3 shows the micro-hardness values for different compositions. It is seen that with the increase in fiber content in the composite, its hardness value improves although the increment is marginal. Figure 4 shows the variation of tensile and flexural strengths of the composites with the fiber content. A gradual increase in tensile strength as well as flexural strength with the weight fraction of fiber is noticed. It clearly indicates

that inclusion of glass fiber improves the load bearing capacity and the ability to withstand bending of the composites. Similar observations have been reported by Harsha et al. [24] for other fiber reinforced thermoplastics such as polyaryletherketone composites. It may be mentioned here that both tensile and flexural strengths are important for recommending a composite for structural applications.

3.2 Steady State Erosion

Erosion wear behavior can be classified as ductile and brittle erosion although this grouping is not definitive. Thermoplastic matrix composites usually show ductile erosion while the thermosetting ones erode in a brittle fashion. Although there is a dispute about this failure classification, Barkoula and Karger-Kocsis [8] argued that the erosive wear behavior strongly depends on the experimental conditions and the composition of the target material. To characterize the morphology of as-received and eroded surfaces and the mode of material removal, the eroded samples are observed under scanning electron microscope. Figure 5 shows the local removal of resin material from the impacted surface resulting in exposure of the fibers to the erodent flux. This micrograph also reveals that due to sand particle impact on fibers there is formation of transverse cracks that break these fibers. Figure 6 presents the microstructure of the same composite with higher magnification. Here the propagation of crack along transverse as well as longitudinal direction is well visualized. On comparing this micro-structure with that of the same composite eroded at a lower impact velocity (45m/s), higher stand-off distance (190 mm) and higher impingement angle (90^0), it can be seen that in the latter case the breaking of glass fibers is more prominent (Figure 7). It appears that cracks have grown on the fibers giving rise to breaking of the fibers into small fragments. Further the cracks have been

annihilated at the fiber matrix interface and seem not to have penetrated through the matrix. Change in impact angle from oblique to normal changes the topography of the damaged surface very significantly. Figure 7 shows the dominance of micro-chipping and micro-cracking phenomena. It can be seen that multiple cracks originate from the point of impact, intersect one another and form wear debris due to brittle fracture in the fiber body. After repetitive impacts, the debris in platelet form are removed and account for the measured wear loss. The occurrence of peak erosion rate at 60^0 impact is understandable. In this case, both abrasion and erosion processes play important roles. The sand particles after impacting, slide on the surface and abrade while dropping down. The wear and subsequently the damage are therefore more than that in the case of normal impact. Marks of micro-ploughing on the ductile polyester matrix region seen in Figure 6 support this argument.

Figure 8 is a plot showing the erosion rates of the composites with three different fiber loadings tested as a function of the angle of impingement (v = 58m/sec). It is quite evident from Figure 8 that the erosion rate initially increases with the impingement angle, attains a peak value at 60^0 and then starts decreasing as the impact angle moves towards 90^0. This trend is exhibited by all the three composites. The Figure 8 also demonstrates that erosion rate increases with the increase in fiber content irrespective of impingement angle. An almost linear variation of the erosion rate with the fiber content can be observed until 60 wt % fiber reinforcement.

In Table 3, the S/N ratio for erosion rate is shown for different combination of factor setting as per experimental design. The S/N ratio for erosion rate is calculated for three repeats under each combination of factor settings. The overall mean for the S/N

ratio of the erosion rate happens to be -16.79 db. Figure 9 shows graphically the effect of the six control factors on erosion rate. The analysis is made using the popular software specifically used for design of experiment applications known as MINITAB 14. Before any attempt is made to use this simple model as a predictor for the measures of performance, the possible interactions between the control factors must be considered. Thus factorial design incorporates a simple means of testing for the presence of the interaction effects. The interaction graphs are shown in Figures 10, 11, 12 and 13. In order to understand a concrete visualization of impact of various factors and their interactions, it is desirable to develop analysis of variance (ANOVA) table to find out the order of significant factors as well as of interactions. Table 4 shows the results of the ANOVA with the erosion rate assuming a level of significance of 5 %. The last column of the table indicates that the probability of significance of major control factors and their interactions. It has been observed that fiber loading (p=0.025), stand-off distance (p=0.134), erodent size (p=0.187), impingement angle (p=0.629) and impact velocity (p=0.790) are significant in the declining order of importance on erosion rate. Among the interactions, the impact velocity × stand-off distance (p=0.052), impact velocity ×fiber loading (p=0.171) and impact velocity ×erodent size (p=0.250) show significance of contribution on the erosion rate. From the above analysis, we conclude that impingement angle (p=0.629) and the interaction between impact velocity and impingement angle (p=0.237) have less significant contribution on erosion rate. Therefore, in order to develop a predictive model impingement angle and interaction between impact velocity and impingement angle can be neglected for further analysis. Analysis of Figures 9-13

leads to determination of an optimum parameter setting $A_2C_1D_1E_1$ causing minimum erosion.

4. Confirmation experiment

The confirmation experiment is the final test in the design of experiment process. The purpose of the confirmation experiment is to validate the conclusions drawn during the analysis phase. The confirmation experiment is performed by conducting a new set of factor settings $A_3C_2D_2E_3$ to predict the erosion rate. The estimated S/N ratio for erosion rate can be calculated with the help of following prediction equation:

$$\hat{\eta}_1 = \overline{T} + (\overline{A}_3 - \overline{T}) + (\overline{C}_2 - \overline{T}) + [(\overline{A}_3\overline{C}_2 - \overline{T}) - (\overline{A}_3 - \overline{T}) - (\overline{C}_2 - \overline{T})] + (\overline{D}_2 - \overline{T}) + [(\overline{A}_3\overline{D}_2 - \overline{T}) - (\overline{A}_3 - \overline{T}) - (\overline{D}_2 - \overline{T})] + (\overline{E}_3 - \overline{T}) + [(\overline{A}_3\overline{E}_3 - \overline{T}) - (\overline{A}_3 - \overline{T}) - (\overline{E}_3 - \overline{T})] \quad (4)$$

$\overline{\eta}_1$	Predicted average
$\overline{T}$	Overall experimental average
$\overline{A}_3, \overline{C}_2, \overline{D}_2$ *and* $\overline{E}_3$	Mean response for factors and interactions at designated levels.

By combining like terms, the equation reduces to

$$\overline{\eta}_1 = \overline{A}_3\overline{C}_2 + \overline{A}_3\overline{D}_2 + \overline{A}_3\overline{E}_3 - 2\overline{A}_3 \quad (5)$$

A new arbitrary combination of factor levels A_3, C_2, D_2, E_3 is used to predict erosion rate through prediction equation and the S/N ratio is found to be $\overline{\eta}_1 = -20.5106\,dB$. An experiment is conducted under factor combination of A_3, C_2, D_2, E_3 and the result is compared with value obtained from the predictive equation as shown in Table 5. The resulting model seems to be capable of predicting erosion rate to a reasonable accuracy. An error of 3.96 % for the S/N ratio of erosion rate is observed. However, the error can be further reduced if the number of measurements is increased.

This validates the development of the mathematical model for predicting the measures of performance based on knowledge of the input parameters.

5. Optimization of Factor Settings for Minimum Erosion Rate

In this study, an attempt is made to derive optimal settings of the control factors for minimization of erosion rate. The single-objective optimization requires quantitative determination of the relationship between erosion rates with combination of control factors. In order to express erosion rate in terms of mathematical model the following form is suggested.

$$Er = K_0 + K_1 \times A + K_2 \times C + K_3 \times D + K_4 \times E + K_5 \times A \times C + K_6 \times A \times D + K_7 \times A \times E \quad (6)$$

Here, *Er* is the performance output term and K_i (i = 0, 1……..7) are the model constants. The constants are calculated using non-linear regression analysis with the help of SYSTAT 7.0 software and the following relation is obtained.

$$Er = -3.446 + 4.302A + 1.462C + 1.034D + 1.613E - 1.287AC - 1.152AD - 2.351AE$$

$$r^2 = 0.96 \quad (7)$$

The correctness of the calculated constants is confirmed because high correlation coefficients (r^2) in the tune of 0.96 are obtained for equation (6) and therefore, the model is quite suitable to use for further analysis. Here, the resultant objective function to be maximized is given as:

Maximize $Z = 1/f$ (8)

f Normalized function for erosion rate

Subjected to constraints:

$$A_{min} \leq A \leq A_{max} \quad (9)$$

$$C_{min} \leq C \leq C_{max} \quad (10)$$

$$D_{min} \leq D \leq D_{max} \quad (11)$$

$$E_{min} \leq E \leq E_{max} \quad (12)$$

The min and max in Eqs.9-12 show the lowest and highest control factor settings used in this study (Table 1).

Genetic algorithm (GA) is used to obtain the optimum value of factor settings for minimizing erosion rate. The computational algorithm is implemented in Turbo C^{++} and run on an IBM Pentium IV machine. Genetic algorithms (GAs) are mathematical optimization techniques that simulate a natural evolution process. They are based on the Darwinian Theory in which the fittest species survive and propagate while the less successful tends to disappear. Genetic algorithm mainly depends on three types of operators viz., reproduction, crossover and mutation. Reproduction is accomplished by copying the best individuals from one generation to the next, what is often called an elitist strategy. The best solution is monotonically improving from one generation to the next. The selected parents are submitted to the crossover operator to produce one or two children. The crossover is carried out with an assigned probability, which is generally rather high. If a number randomly sampled is inferior to the probability, the crossover is performed. The genetic mutation introduces diversity in the population by an occasional random replacement of the individuals. The mutation is performed based on an assigned probability. A random number is used to determine if a new individual will be produced to substitute the one generated by crossover. The mutation procedure consists of replacing one of the decision variable values of an individual while keeping the remaining variables unchanged. The replaced variable is randomly chosen and its new value is calculated by randomly sampling within its specific range.

In genetic optimization, population size, probability of crossover and mutation are set at 50, 75 %, and 5 % respectively. Number of generation is varied till the output is converged. Table 6 shows the optimum conditions of the control factors with optimum performance output that suggest best combination of set of input control factors. The pattern of convergence of performance output with number of generations is shown in Figure 14.

6. Conclusions

Based on the present study on solid particle erosion of glass fiber reinforced polyester at various parameter settings of impact velocity, fiber loading, erodent size, impingement angle and stand-off distance, the conclusions can be drawn as follows.

1. Solid particle erosion characteristics of these composites can be successfully analyzed using Taguchi experimental design scheme. Taguchi method provides a simple, systematic and efficient methodology for the optimization of the control factors and their interactions.
2. The results indicate that fiber loading, stand-off distance, erodent size, impingement angle and impact velocity are the significant factors in a declining sequence affecting the erosion wear rate. Although the effect of impact velocity is less compared to other factors, it cannot be ignored because it shows significant interaction with stand-off distance, fiber loading and erodent size. An optimal parameter combination is determined, which leads to minimization of material loss due to erosion.
3. Literature on solid particle erosion on PMCs reveals that influence of impact velocity is quite significant on erosion rate. Undoubtedly, the fact is true but

under the influence of other process parameters, impact velocity becomes comparatively less important.

4. Further, interactions among the impact velocity × stand-off distance, impact velocity × fiber loading and impact velocity × erodent size in the order of priority exhibits significant influence on erosion rate.
5. The composites exhibit semi-ductile erosion characteristics with the peak erosion wear occurring at 60^0 impingement angle. This nature has been explained by analyzing the possible damage mechanism with the help of SEM micrographs. It is concluded that the inclusion of brittle fibers in polyester matrix is responsible for this semi-ductility.
6. The rationale behind the use of genetic algorithm lies in the fact that genetic algorithm has the capability to find the global optimal parameter settings, whereas the traditional optimization techniques normally stick up at the local optimum values. The optimum settings are found to be impact velocity = 57.942m/sec, fiber loading= 52.26%, erodent size = 778.4μm and stand-off distance = 180.72 mm resulting erosion rate = 7.6910 mg/kg as far as present experimental conditions are concerned.
7. In future, the study can be extended to samples of different work materials, use of fillers and hybrid optimization techniques.

References

1. H. Wahl, F. Hartenstein, Strahlverschleiss, Frankh'sche Verlagshandlung, Stuttgart, (1946).
2. J.G.A. Bitter, A study of erosion phenomena; Part II, Wear 6 (1963). 169-190.
3. E. Raask, Wear 13 (1968) 303-313.
4. W.A. Hibbert, J. Roy, Aero. Soc., 69 (1965) 769-776.
5. K.V.Pool, C.K.H Dharan, I. Finnie, Erosion wear of composite materials, Wear 107(1986) 1-12.
6. S.M Kulkarni, Kishore, Influence of matrix modification on the solid particle erosion of glass/epoxy composites, Polym. Polym.Composites, 9 (2001) 25–30.
7. H.A Aglan, Jr T.A Chenock, Erosion damage features of polyimide thermoset composites, SAMPE Quart., (1993). 41–47.
8. N.M. Barkoula, J. Karger-Kocsis, Effect of fiber content and relative fiber-orientation on the solid particle erosion of GF/PP composite, Wear 252 (2002) 80-87.
9. U.S. Tewari, A.P. Harsha, A.M. Hager, K. Friedrich, Solid particle erosion of unidirectional carbon fiber reinforced polyetheretherketone composites, Wear 252 (2002) 992-1000.
10. A. Häger, K. Friedrich, Y.A. Dzenis, S.A. Paipetis, Study of erosion wear of advanced polymer composites, In: K. Street, B.C. Whistler(Eds.), Proceedings of the ICCM-10, Canada Wood head Publishing Ltd., Cambridge, (1995) 155–162,
11. N. Miyazaki, T. Takeda, Solid particle erosion of fiber reinforced plastic, J.compos Mater, 27 (1993) 21-31.

12. G. P. Tilly, W. Sage, The interaction of particle and material behaviour in erosion process, Wear 16 (1970) 447-65.
13. B.A Lindsley, A.R. Marder, The effect of velocity on the solid particle erosion rate of alloys, Wear 225-229 (1999) 510-516,
14. G. Sundararajan, Manish Roy, Solid particle erosion behaviour of metallic materials at room and elevated temperatures, Tribology International, 30 (1997) 339-359.
15. S.S. Mahapatra and Amar. Patnaik, Optimization of Wire Electrical Discharge Machining (WEDM) process Parameters using Genetic Algorithm, Int. J.Adv. Manuf. Technol. (2006a) DOI.10.1007/s00170-006-0672-6.
16. S.S. Mahapatra and Amar. Patnaik, Optimization of Parameter Combinations in Wire Electrical Discharge Machining using Taguchi method, Indian journal of engineering & material sciences, 13 (2006c) 494-502
17. S.S. Mahapatra, and Amar. Patnaik, Development and Analysis of Wear Resistance Model for Composites of Aluminium Reinforced with Red mud, The journal of Solid Waste Technology and Management 32 (1) (2006d) 28-35.
18. S.S. Mahapatra and Amar. Patnaik, Determination of Optimal Parameters Settings in Wire Electrical Discharge Machining (WEDM) Process using Taguchi method, Journal of Institution of Engineering (India), 187 (2006e) 16-24.
19. S.S Mahapatra and Amar. Patnaik, Parametric Optimization of Wire Electrical Discharge Machining (WEDM) Process using Taguchi method, Journal of the Brazilian Society of Mechanical Sciences, 28(4) (2007) 423-430.

20. S.S. Mahapatra and Amar. Patnaik, Parametric Analysis and Optimization of Drilling of Metal Matrix Composites based on the Taguchi Method, The International Journal for Manufacturing Science and Technology, 8 (2006b) 5-12.
21. Amar Patnaik, Alok Satapathy, S.S. Mahapatra, R.R.Dash., Modeling and Prediction of Erosion Response of Glass Reinforced Polyester-Flyash Composites, Journal of Reinforced Plastics and Composites (2007) (In press).
22. S. Phadke. Madhav, Quality Engineering using Robust Design, Prentice Hall, Eaglewood Cliffs, New Jersey, (1989).
23. S. P. Glen, Taguchi methods: A hands on approach, Addison-Wesley, New York. (1993).
24. A.P.Harsha. U.S.Tewari, B.Venkatraman, Solid particle erosion behavior of various polyaryletherketone composites, Wear 254 (2003) 693-712.

List of Tables

Table 1 Levels of the variables used in the experiment

Control factor	Level			
	I	II	III	Units
A: Impact Velocity	32	45	58	m/sec
B: Impingement Angle	30	60	90	degree
C: Fiber loading	40	50	60	%
D: Erodent size	450	600	800	µm
E: Stand off distance	120	160	190	mm

Table 2 Orthogonal array for L_{27} (3^{13}) Taguchi Design

$L_{27}(3^{13})$	1	2	3	4	5	6	7	8	9	10	11	12	13
	A	B	$(AxB)_1$	$(AxB)_2$	C	$(AxC)_1$	$(AxC)_2$	D	$(AxD)_1$	$(AxD)_2$	E	$(AxE)_1$	$(AxE)_2$
1	1	1	1	1	1	1	1	1	1	1	1	1	1
2	1	1	1	1	2	2	2	2	2	2	2	2	2
3	1	1	1	1	3	3	3	3	3	3	3	3	3
4	1	2	2	2	1	1	1	2	2	2	3	3	3
5	1	2	2	2	2	2	2	3	3	3	1	1	1
6	1	2	2	2	3	3	3	1	1	1	2	2	2
7	1	3	3	3	1	1	1	3	3	3	2	2	2
8	1	3	3	3	2	2	2	1	1	1	3	3	3
9	1	3	3	3	3	3	3	2	2	2	1	1	1
10	2	1	2	3	1	2	3	1	2	3	1	2	3
11	2	1	2	3	2	3	1	2	3	1	2	3	1
12	2	1	2	3	3	1	2	3	1	2	3	1	2
13	2	2	3	1	1	2	3	2	3	1	3	1	2
14	2	2	3	1	2	3	1	3	1	2	1	2	3
15	2	2	3	1	3	1	2	1	2	3	2	3	1
16	2	3	1	2	1	2	3	3	1	2	2	3	1
17	2	3	1	2	2	3	1	1	2	3	3	1	2
18	2	3	1	2	3	1	2	2	3	1	1	2	3
19	3	1	3	2	1	3	2	1	3	2	1	3	2
20	3	1	3	2	2	1	3	2	1	3	2	1	3
21	3	1	3	2	3	2	1	3	2	1	3	2	1
22	3	2	1	3	1	3	2	2	1	3	3	2	1
23	3	2	1	3	2	1	3	3	2	1	1	3	2
24	3	2	1	3	3	2	1	1	3	2	2	1	3
25	3	3	2	1	1	3	2	3	2	1	2	1	3
26	3	3	2	1	2	1	3	1	3	2	3	2	1
27	3	3	2	1	3	2	1	2	1	3	1	3	2

Table 3 Experimental design using L_{27} orthogonal array

Sl. No.	Impact Velocity(A) m/sec	Impingement angle (B)Degree	Fiber loading (C)%	Erodent size (D) µm	Stand-off distance (E) mm	Erosion rate(Er) mg/kg	S/N Ratio (db)
1	32	30	40	450	120	7.218	-17.1683
2	32	30	50	600	160	8.749	-18.8392
3	32	30	60	800	190	36.070	-31.1429
4	32	60	40	600	190	7.328	-17.2997
5	32	60	50	800	120	9.937	-19.9451
6	32	60	60	450	160	8.607	-18.6970
7	32	90	40	800	160	6.164	-15.7973
8	32	90	50	450	190	3.562	-11.0339
9	32	90	60	600	120	13.820	-22.8102
10	45	30	40	450	120	6.492	-16.2476
11	45	30	50	600	160	5.937	-15.4713
12	45	30	60	800	190	8.455	-18.5423
13	45	60	40	600	190	3.164	-10.0047
14	45	60	50	800	120	6.562	-16.3407
15	45	60	60	450	160	6.911	-16.7908
16	45	90	40	800	160	5.274	-14.4428
17	45	90	50	450	190	4.749	-13.5320
18	45	90	60	600	120	27.640	-28.8308
19	58	30	40	450	120	12.350	-21.8333
20	58	30	50	600	160	11.870	-21.4890
21	58	30	60	800	190	4.607	-13.2684
22	58	60	40	600	190	4.164	-12.3902
23	58	60	50	800	120	27.310	-28.7264
24	58	60	60	450	160	6.911	-16.7908
25	58	90	40	800	160	3.164	-10.0047
26	58	90	50	450	190	10.680	-20.5714
27	58	90	60	600	120	12.670	-22.0555

Table 4 ANOVA table for erosion rate

Source	DF	Seq SS	Adj SS	Seq MS	F	P
A	1	3.32	240.80	3.32	0.07	0.790
B	1	10.93	65.84	10.93	0.24	0.629
C	1	275.13	173.12	275.13	6.09	0.025
D	1	85.30	98.33	85.30	1.89	0.187
E	1	111.79	125.78	111.79	2.47	0.134
A*B	1	57.11	57.11	57.11	1.26	0.277
A*C	1	92.28	92.28	92.28	2.04	0.171
A*D	1	64.16	64.16	64.16	1.42	0.250
A*E	1	196.47	196.47	196.47	4.35	0.052
Error	17	768.33	768.33	45.20		
Total	26	1664.82				

Table 5 Results of the confirmation experiments for Erosion rate

	Optimal control parameters	
	Prediction	Experimental
Level	$A_3C_2D_2E_3$	$A_3C_2D_2E_3$
S/N ratio for Erosion rate (db)	-19.6984	-20.5106

Table 6 Optimum conditions for performance output

Control factors and Performance characteristics	Optimum conditions
A: Impact velocity (m/sec)	57.942
C: Fiber loading (%)	52.26
D: Erodent size (μm)	778.4
E: Stand of distance (mm)	180.72
Erosion Rate (mg/kg)	7.6910

List of Figure(s)

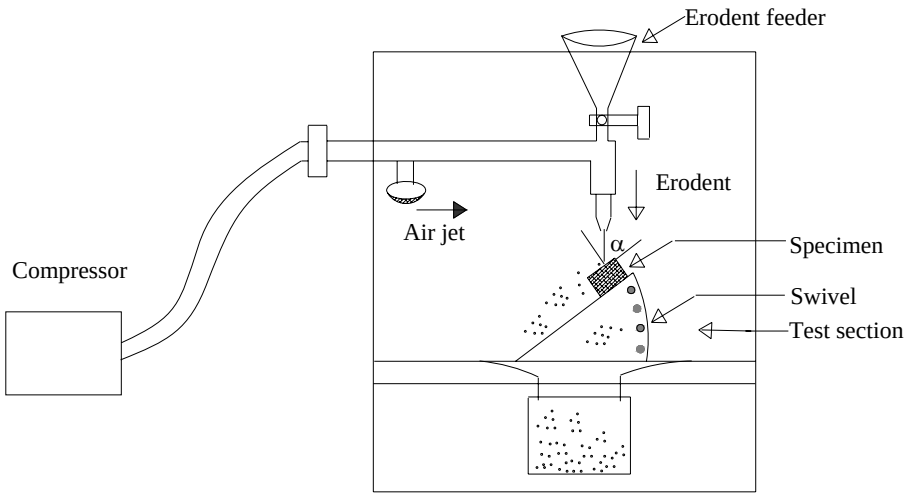

Figure 1 A schematic diagram of the erosion test rig.

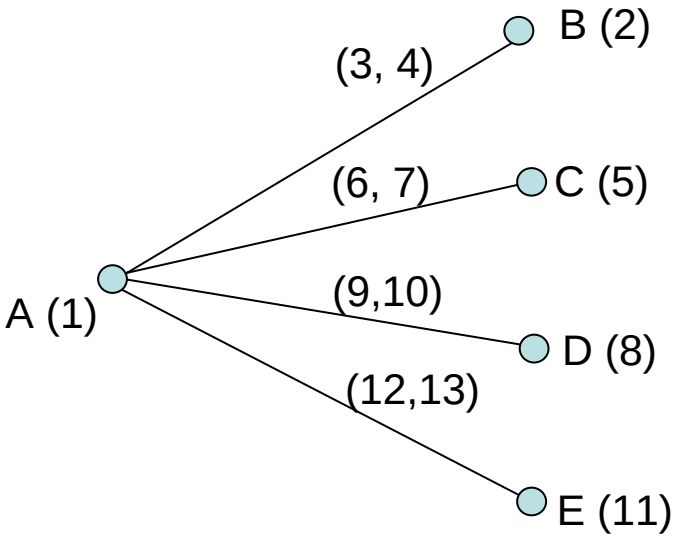

Figure 2 Linear graphs for L_{27} array

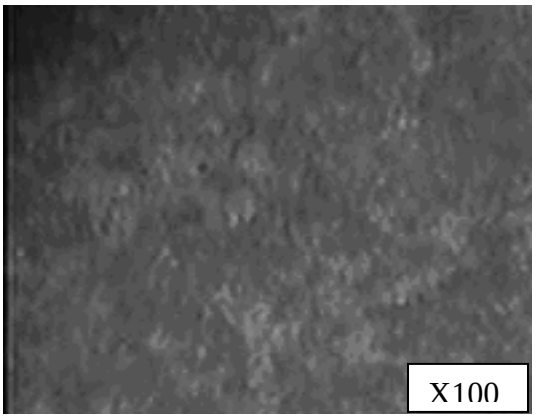

Figure 3 Optical micro-structure of glass polyester composite (50 % fiber loading)

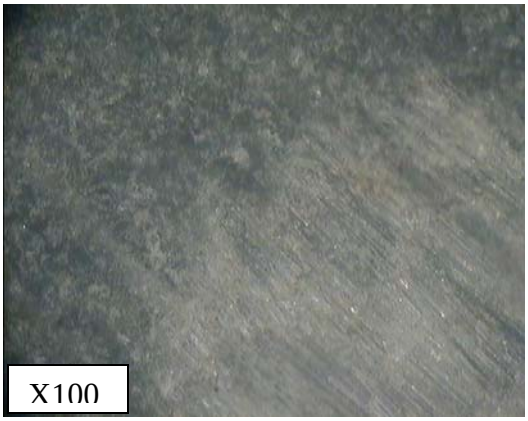

Figure 4. Optical micro-structure of typical eroded surface (50 % fiber loading, 800µm erodent size and 60^0 impingement angle)

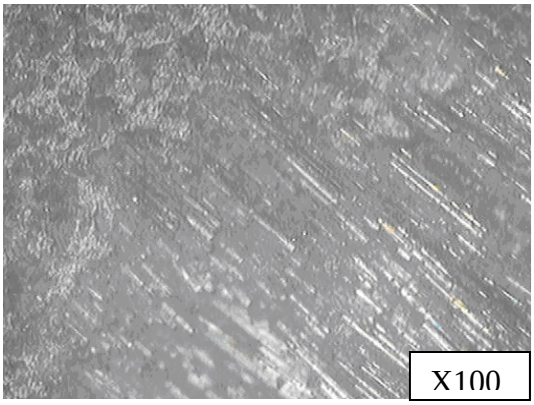

Figure 5 Optical micro-structure of higher magnification eroded surface.

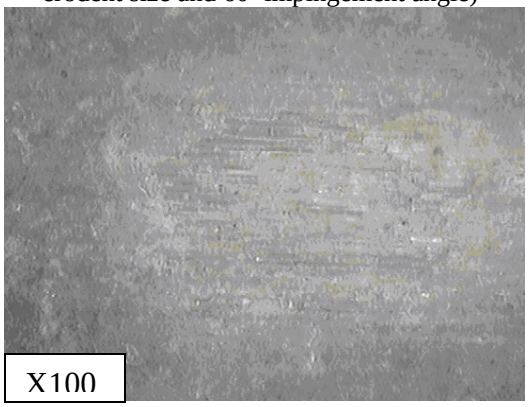

Figure 6. Optical micro-structure of composite (800µm erodent size and impingement angle 90^0)

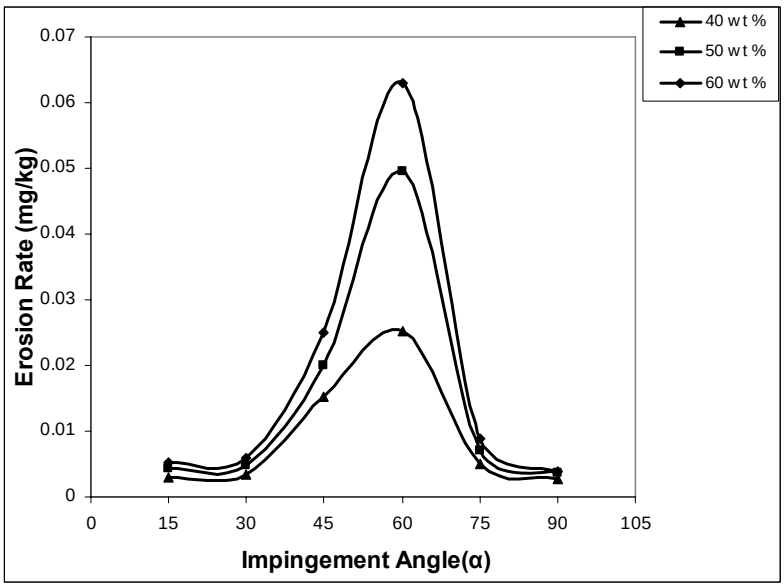

Figure 7 Erosion rate vs. Angle of impingement for different fiber loading

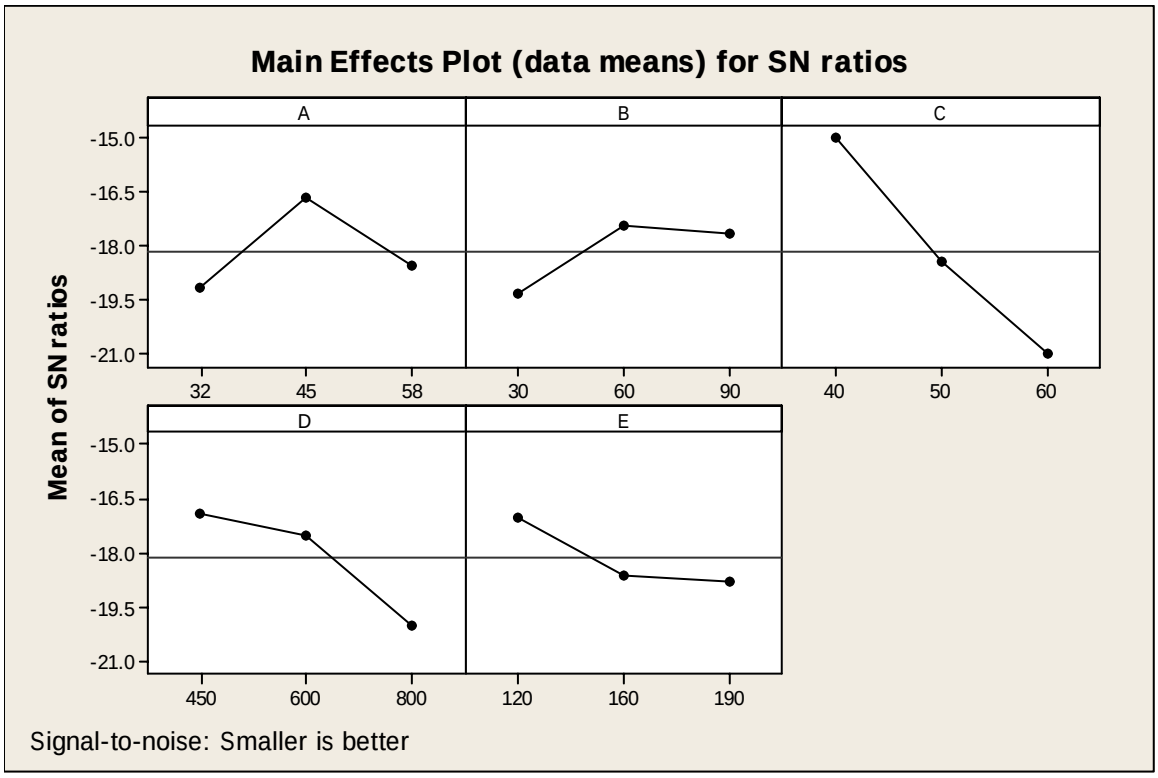

Figure 8 Effect of control factors on erosion rate

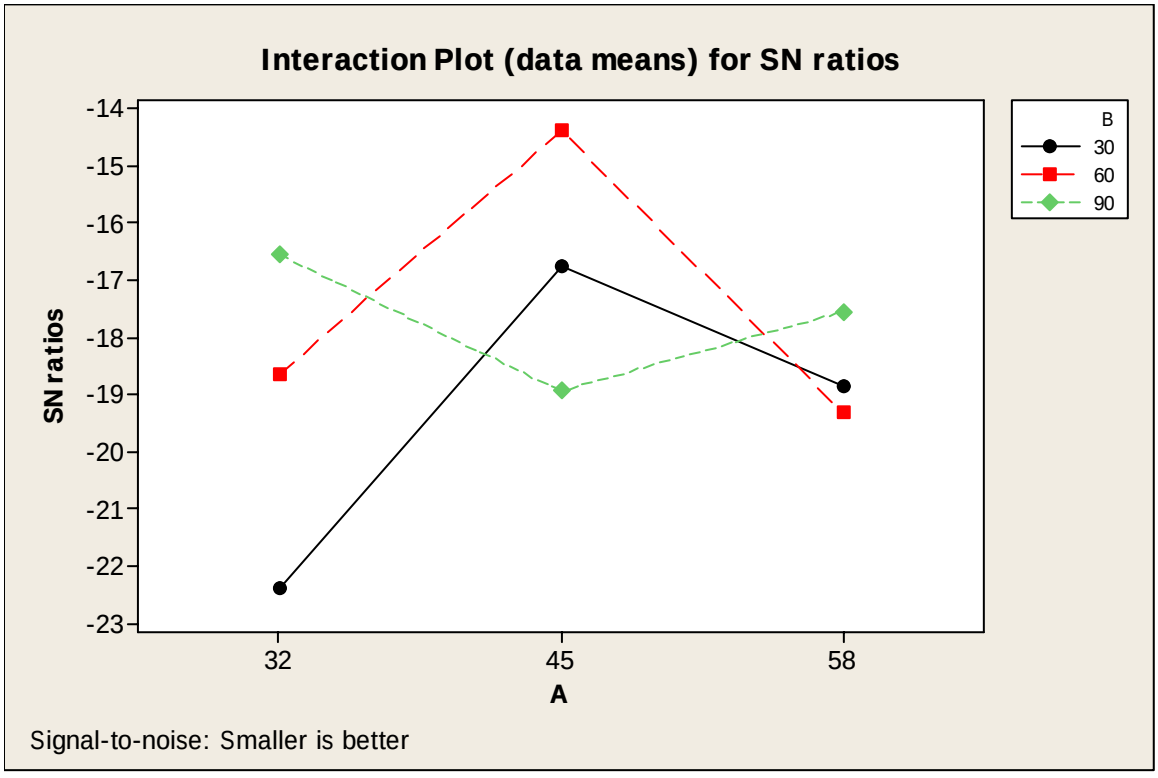

Figure 9 Interaction graph between A×B for erosion rate

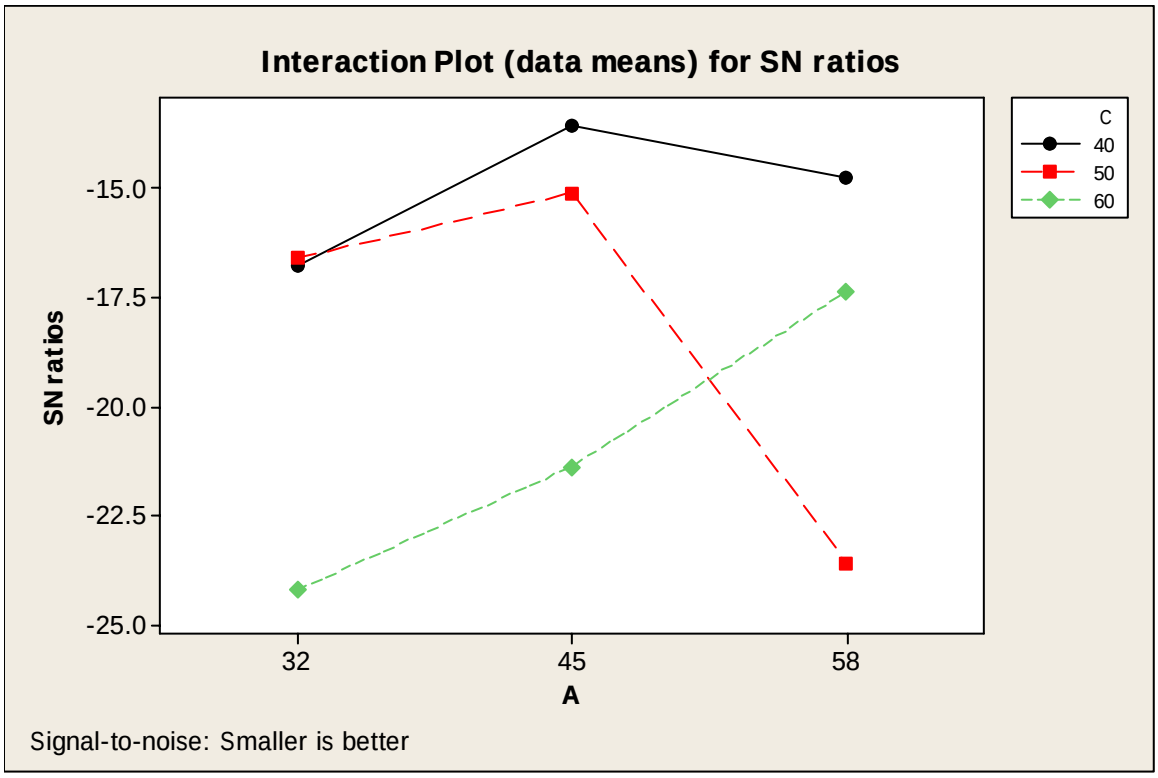

Figure 10 Interaction graph between A×C for erosion rate

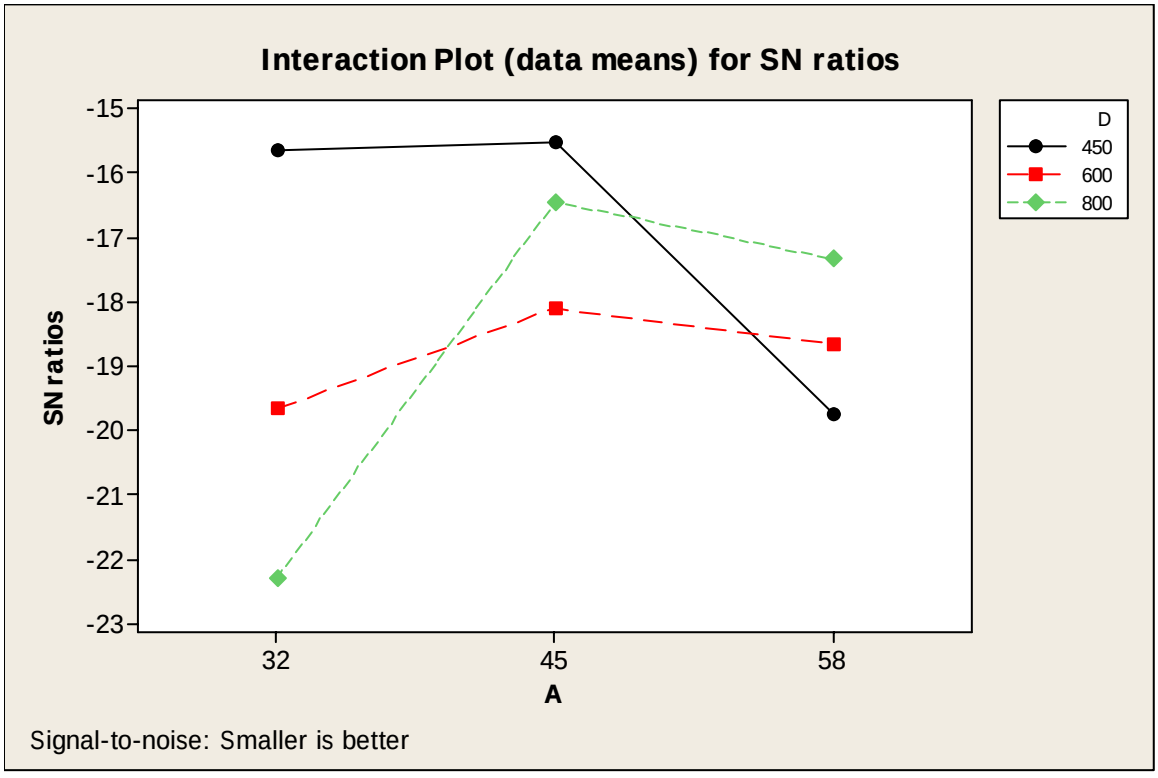

Figure 11 Interaction graph between A×D for erosion rate

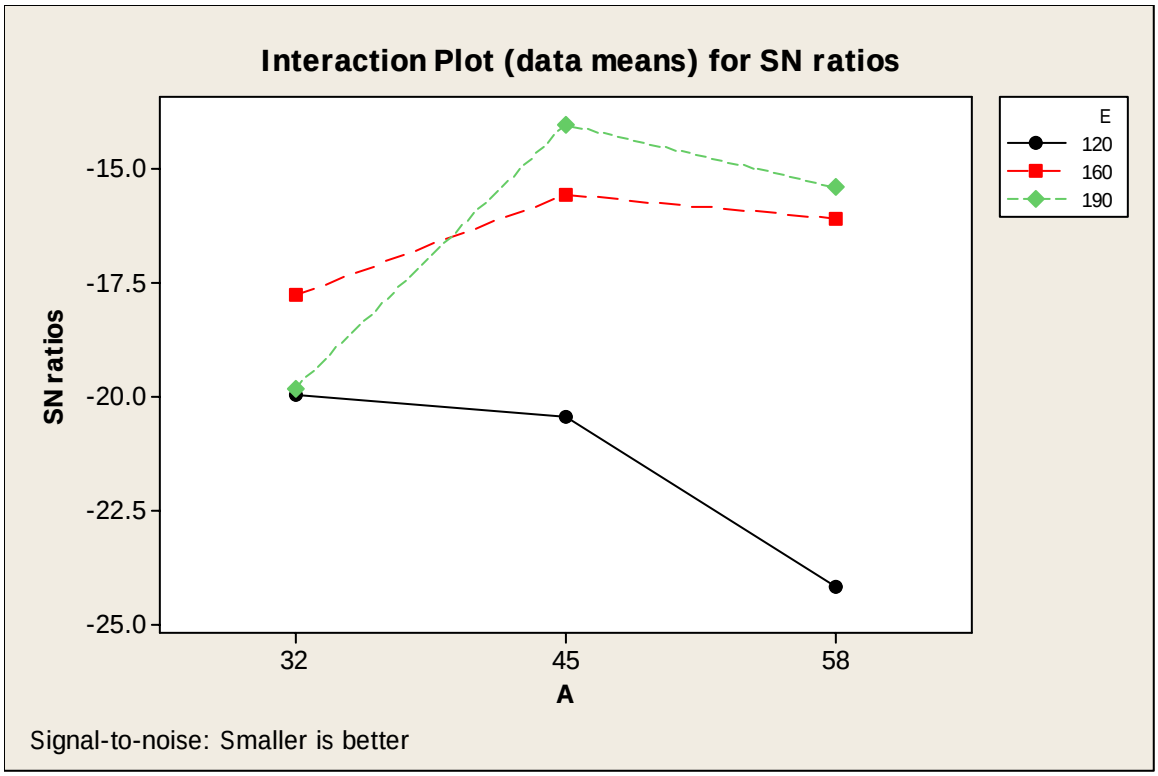

Figure 12 Interaction graph between A×E for erosion rate

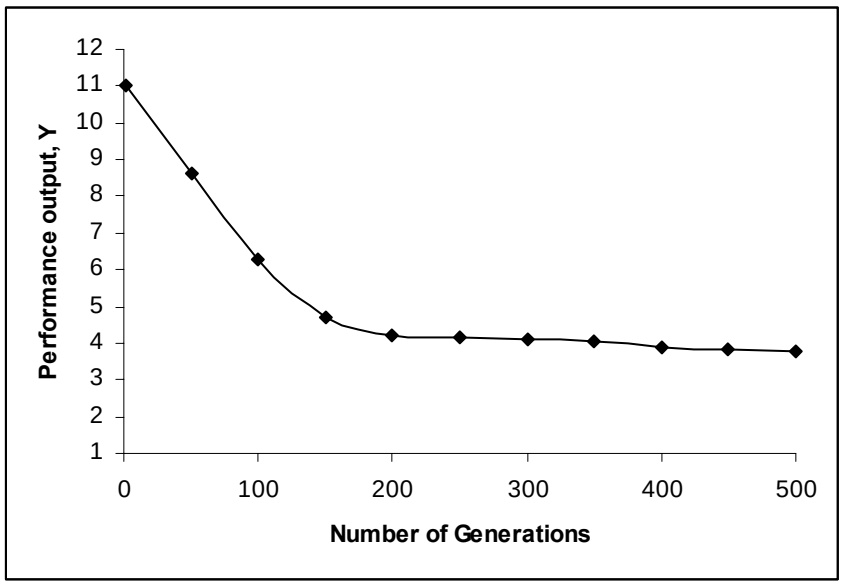

Figure 13 Convergence Curve